J. Electrochem. Sci. Eng. **13(5)** (2023) 771-782; http://dx.doi.org/10.5599/jese.1643

Open Access : : ISSN 1847-9286
https://pub.iapchem.org/ojs/index.php/JESE

Original scientific paper

Reduced graphene oxide as efficient carbon support for Pd-based ethanol oxidation catalysts in alkaline media

Sigrid Wolf[1,✉], Michaela Roschger[1], Boštjan Genorio[2], Nejc Hodnik[3], Matija Gatalo[3], Francisco Ruiz-Zepeda[3] and Viktor Hacker[1]

[1]*Institute of Chemical Engineering and Environmental Technology, Graz University of Technology, Inffeldgasse 25/C, 8010 Graz, Austria*
[2]*Faculty of Chemistry and Chemical Technology, University of Ljubljana, Večna pot 113, 1000 Ljubljana, Slovenia*
[3]*Department of Materials Chemistry, National Institute of Chemistry, Hajdrihova 19, 1000 Ljubljana, Slovenia*

Corresponding author: ✉*sigrid.wolf@tugraz.at*

Received: December 21, 2022; Accepted: January 24, 2023; Published: February 8, 2023

Abstract

The sluggish kinetics of the ethanol oxidation reaction (EOR) and the related development of low-cost, highly active and stable anode catalysts still remains the major challenge in alkaline direct ethanol fuel cells (ADEFCs). In this respect, we synthesized a PdNiBi nanocatalyst on reduced graphene oxide (rGO) via a facile synthesis method. The prepared composite catalyst was physicochemically characterized by SEM, STEM, EDX, ICP-OES and XRD to analyze the morphology, particle distribution and size, elemental composition and structure. The electrochemical activity and stability towards EOR in alkaline media were examined using the thin-film rotating disk electrode technique. The results reveal well-dispersed and strongly anchored nanoparticles on the rGO support, providing abundant active sites. The PdNiBi/rGO presents a higher EOR activity and stability compared to a commercial Pd/C ascribed to a high ECSA and synergistic effects between Pd, Ni and Bi and the rGO material. These findings suggest PdNiBi/rGO as a promising anode catalyst in ADEFC applications.

Keywords

Synergistic effects; electrochemical active surface area; rotating disk electrode; alkaline direct ethanol fuel cell

Introduction

Fuel cells have emerged as one of the most promising renewable energy technologies of the future, as they convert chemical energy directly into electrical energy [1,2]. Alkaline direct ethanol fuel cells (ADEFCs) have gained significance among the various fuel cell types, especially for portable and transportation applications, as they have a high theoretical energy density (8 kWh kg^{-1}), they

are environmentally friendly, and ethanol can be easily handled compared to other fuels such as hydrogen [3,4]. Ethanol has proven significant advantages over methanol as it can be produced from agricultural products, is non-toxic and features a lower crossover from the anode to the cathode [4,5]. However, one of the major problems of ADEFCs remains the development of cost-efficient, highly active and stable electrocatalysts for the ethanol oxidation reaction (EOR) at the anode. Pd-based catalysts are currently reported to be most suitable and show better EOR performance in alkaline media than their Pt counterparts [2,6]. The C-C bond of ethanol is difficult to break and the EOR does not proceed via a complete oxidation (equation (1)) with the formation of CO_2 and 12 e^-, but via incomplete oxidation to acetate and 4 e^- (equation (2)) [1,4].

Complete oxidation: $CH_3CH_2OH + 12\ OH^- \rightarrow 2\ CO_2 + 9\ H_2O + 12\ e^-$ (1)

Incomplete oxidation: $CH_3CH_2OH + 5\ OH^- \rightarrow CH_3COO^- + 4\ H_2O + 4\ e^-$ (2)

To overcome this problem, alloying Pd with oxophilic co-catalyst elements such as Ni, Bi, Cd or Co is very effective for increasing the EOR activity and stability due to enhanced -OH^- adsorption while reducing costs [7-11]. Deposition of the metal nanoparticles on a suitable support material offers another possibility to increase the efficiency of such catalysts, as it features the capability to control the size, distribution, morphology and stability of the immobilized particles. Carbon powders such as carbon black, carbon nanotubes or graphene are commonly used as support [4,8,11]. Among these carbon materials, reduced graphene oxide (rGO) has proven to be particularly suitable for this purpose, as its unique sp^2-hybridized carbon structure provides properties such as a large specific surface area (SSA), high thermal and chemical stability, and excellent electronic conductivity. Usually rGO still retains important oxygen-containing functionalities (*e.g.* epoxy, hydroxyl, and carboxyl groups), causing strong C-O-metal bridges that enhance the stability and prevent agglomeration of the nanoparticles [4,6,8,12]. Krishna *et al.* [13] have described, for example, that a Pd@Ni_xB/RGO nanocomposite exhibited improved catalytic activity and stability compared with the unsupported nanoparticles. Another study by Alfi *et al.* [9] also showed that a Pd-Cd/rGO catalyst outperforms the commercial Pd/C in terms of EOR performance. A combination of adding oxophilic co-catalysts to the Pd active material and the deposition on a suitable support material such as rGO therefore appears to be a promising approach for the development of highly active and stable EOR catalysts.

Based on the above findings, in this work we synthesized a composite catalyst of PdNiBi nanoparticles on rGO for the first time and investigated the electrochemical activity and stability towards EOR in alkaline media. The PdNiBi/rGO catalyst was comprehensively characterized by various physicochemical techniques, which confirmed the successful deposition of the metal particles on the rGO support. Finally, the electrochemical rotating disk electrode (RDE) experiments revealed a promising catalytic EOR performance of the prepared nanocomposite attributed to synergistic effects between Pd, Ni and Bi and the rGO support material.

Experimental

Materials

The following chemicals were used for material preparation and electrochemical tests without further purification: graphene oxide (GO) precursor (Timrex KS44) was acquired from Imerys (Bodio, Switzerland), sodium borohydride ($NaBH_4$, 97 %) was delivered by Alfa Aesar (Haverhill, MA, USA) and sodium hydroxide (NaOH, ≥98 %, ACS, pellets) was purchased from Honeywell Fluka (Charlotte, NC, USA). Hydrazine hydrate ($N_2H_4{\cdot}H_2O$, reagent grade), palladium chloride ($PdCl_2$, anhydrous, 59-60 % Pd basis), nickel(II) nitrate hexahydrate ($Ni(NO_3)_2{\cdot}6H_2O$, 99 % trace metal basis), bismuth(III) chloride

($BiCl_3$, reagent grade, ≥98 %) and potassium hydroxide (KOH, 1.0 M Fixanal 1 L Ampoule) were purchased from Sigma-Aldrich (Darmstadt, Germany). Hydrochloric acid (HCl, ROTIPURAN®37 % fuming, *p.a.*, ACS, ISO), ethanol (EtOH, 99.9 % *p.a.*) and isopropyl alcohol (2-propanol, ≥99.9 %, UV/IR-grade) were supplied by Carl Roth (Karlsruhe, Germany). Nafion™ Solution (5 wt.% in H_2O) from Quintech (Göppingen, Germany) and an alumina suspension (Al_2O_3, 0.05 µm particle size) from MasterPrep® Bühler (Lake Bluff, IL, USA) were used. All solutions were prepared with ultrapure water (Barnstead NANOpureWater Purification System, ~18 MΩ cm). A commercial Pd/C (40 wt.%) from Fuel Cell Store (College Station, TX, USA) was used as a benchmark for the electrochemical results.

Catalyst preparation

The preparation of rGO was carried out using a previously published chemical reduction method [5,14]. First, the GO precursor and ultrapure water were mixed in a 2 L-round bottom flask. The dispersion was slowly heated to 100 °C under reflux and stirred at 550 rpm using an oil bath and a PTFE magnetic stir bar. Hydrazine hydrate was then slowly added to perform the reduction process at 105 °C for 24 h. After successful reduction, indicated by a color change from brown to black, filtration of the hot reaction mixture and intensive washing with hot ultrapure water and ethanol was performed. The rGO was obtained by drying at air (24 h) and subsequently under vacuum at 80 °C (overnight) and was used as catalyst support material without further purification.

The PdNiBi/rGO (40 wt.% of metal and 60 wt.% of carbon support) composite catalyst was synthesized according to the modified instant reduction method [7,15]. The as-prepared rGO was dispersed in ultrapure water under a nitrogen atmosphere and ice cooling using an ultrasonic probe (Hilscher, UP440s). Afterwards, the following three metal precursor salt solutions were added to the rGO dispersion: $PdCl_2$ and $Ni(NO_3)_2{\cdot}6H_2O$ were both mixed with ultrapure water and 1 M HCl and $BiCl_3$ was dissolved in ultrapure water and a few drops of HCl (concentrated). The pH was then adjusted to 10, an aqueous solution of $NaBH_4$ (in ultrapure water and 1 M NaOH) was slowly added and the reduction was carried out at 60 °C for 4 h. Finally, the precipitate was filtered, washed with ultrapure water and dried at 40 °C for 24 h.

Characterization

The morphology and particle size of the metal nanoparticles were studied in a probe Cs-corrected Jeol ARM 200 CF scanning transmission electron microscope (STEM) system equipped with an SDD Jeol Centuria Energy-dispersive X-ray (EDX) spectrometer at 80 kV. For the sample preparation, the catalyst was dispersed in ethanol, dropped on a Cu-grid and dried. Scanning electron microscopy (SEM) was carried out on a Zeiss Ultra+ field emission scanning electron microscope at 1 kV with a secondary electron detector to further analyze the catalyst morphology. A conductive carbon tape on an Al stub served as a sample holder. EDX spectroscopy was performed at 7 kV within the SEM using an SDD X-MAX 50 EDX spectrometer to determine the elemental composition. Metal concentration was additionally examined by inductively coupled plasma optical emission spectrometry (ICP-OES) on an Acros SOP system by Spectro using detection wavelengths of 223.061 (Bi), 231.604 (Ni) and 340.458 (Pd). The sample preparation was as follows: microwave-assisted pressurized acid digestion on a Multiwave 3000 of the sample (~10 mg) in 7 mL of concentrated HNO_3, 0.2 mL $HClO_4$ and 0.2 mL HF (40 %) was done at 195 °C and 1500 W for 25 min. The crystal structure of the composite catalyst was characterized by X-ray diffractometry (XRD). The measurement was conducted on a PANalytical X'Pert PRO MPD diffractometer with a fully opened X'Celerator detector using a Cu Kα1 radiation (λ = 0.15406 nm) within a 2θ range from 20 to 60° and a step size of 0.034° step per 100 s. The sample was placed on a zero-background Si holder.

Electrochemical measurements

Electrochemical characterization of the Pd-based composite catalysts was performed in a three-electrode cell by using a rotating disk electrode (RDE) and a workstation from Pine Research Instrumentation. A glassy carbon (GC) disk electrode (AFE5T0GC) coated with a thin film of the catalyst material, a platinized titanium rod (Bank Elektronik - Intelligent Controls GmbH) and a reversible hydrogen electrode (RHE, HydroFlex®, gaskatel) were used as working, counter and reference electrode, respectively.

The GC disk was polished with an Al_2O_3 suspension (0.5 µm) and rinsed with ultrapure water before the catalyst layer was applied. 10 µL of an ultrasonically dispersed (30 min) ink containing 8.1 mg catalyst powder, 1.75 mL 2-propanol, 0.737 mL ultrapure water and 13 µL of a Nafion solution (5 wt.%) were pipetted onto the GC disk (0.196 cm^{-2}) and dried at 700 rpm for 1 h to form a thin-film with a final Pd loading of 56 µg cm^{-2}.

Measurements were carried out using a Reference 600TM potentiostat/galvanostat/ZRA and software from GAMRY Instruments was utilized for data analysis. A constant temperature of 30 °C and de-aerated (N_2-purging for 30 min) electrolyte solution was used for all experiments. First, cyclic voltammograms (CVs) in 1 M KOH at 50 mV s^{-1} (until a reproducible CV curve was obtained) for cleaning purpose and at 10 mV s^{-1} for the analysis of the redox processes were recorded in a potential range from 0.05 to 1.50 V *vs.* RHE. Then, CVs at a scan rate of 10 mV s^{-1} were conducted from 0.05 to 1.20 V *vs.* RHE in 1 M KOH (base CVs) and a mixture of 1 M KOH / 1 M EtOH to evaluate the electrochemical active surface area (ECSA) and the EOR activity of the Pd-based nanocatalysts, respectively. For each measurement (except cleaning CVs) three cycles were performed and the third was used for investigation. The CVs for the EOR were corrected with the base CVs to exclude the redox processes not linked to EOR. Chronoamperometry (CA) tests were carried out in the ethanol-containing electrolyte solution (1 M KOH / 1 M EtOH) at a potential of 0.83 V *vs.* RHE for 3600 s to examine the catalytic EOR stability.

Results and discussion

Structural, morphological and elemental characteristics of PdNiBi/rGO

Comprehensive physicochemical characterization of the prepared PdNiBi/rGO composite was performed to analyze the morphology, particle size and distribution of the nanoparticles, the elemental composition and the crystal structure.

Figure 1 shows the STEM, SEM and EDX elemental mapping images of the catalyst. The STEM images in Figure 1a-c and 1e-g indicate metal nanoparticles anchored on the rGO sheets and the SEM image of PdNiBi/rGO (Figure 1d) evidences the two-dimensional wrinkled sheet morphology of the sample [2,6,9]. The particles are uniformly and well dispersed and only a few agglomerates are noticed. The remaining oxygen-containing functional groups, such as hydroxyl (-OH) of the rGO support, are crucial for holding the metal particles by strong C-O-M bridges and act as a capping agent to prevent strong agglomeration and ensure the formation of very small particles [13]. Therefore, a large specific surface area and abundant active sites are provided. The particle size distribution (PSD) is shown in the inset of Figure 1f. The statistical analysis results in an average particle diameter of 2.6 nm. From the EDX elemental mapping (Figure 1h), the presence of Pd, Ni and Bi and the homogeneous distribution of the elements can be proved. The elemental composition of PdNiBi/rGO determined by EDX and ICP-MS is given in Table 1.

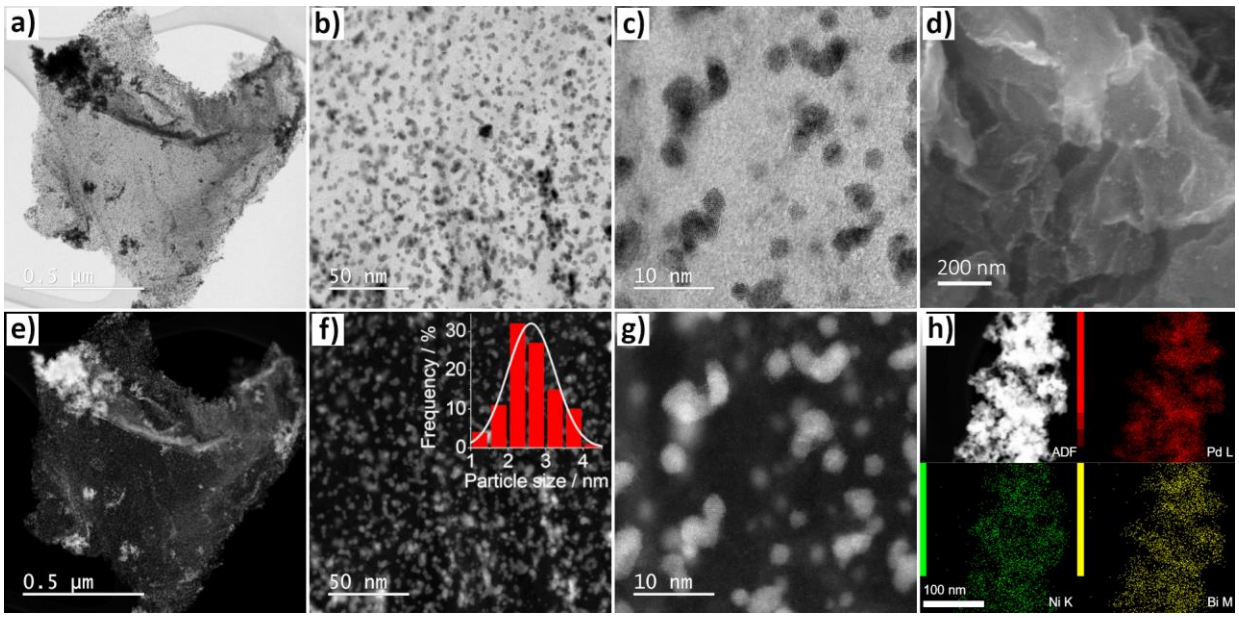

Figure 1. *(a,b,c,e,f,g) BF and ADF STEM (with PSD inset), (d) SEM and (h) EDX elemental mapping images of PdNiBi/rGO*

Table 1. *Elemental composition of PdNiBi/rGO derived by EDX or ICP-OES compared with calculated values*

Material	Content, wt.%				
	C	O	Pd	Ni	Bi
Calculated	60.0	-	33.9	2.2	3.9
EDX	46.3	12.0	34.5	2.5	3.2
ICP-OES	-	-	27.7	2.0	3.7

The ratio between support and the active metal material is approx. 60:40. It can also be observed that the support material is composed of C (46.3 wt.%) and O (12.0 wt.%), which confirms the presence of the oxygen-containing functional groups within the rGO. The active material (~40 wt.%) is composed of Pd, Ni and Bi and is well comparable with the calculated values. This results in an atomic proportion of approx. 85 wt.% Pd, 10 wt.% Ni and 5 wt.% Bi (calculated from the active material only).

The crystal structure of the PdNiBi/rGO composite was analyzed by XRD. The XRD pattern of the prepared material and comparison with graphite (ICSD #18838) and Pd (ICSD #64922) standard data is shown in Figure 2.

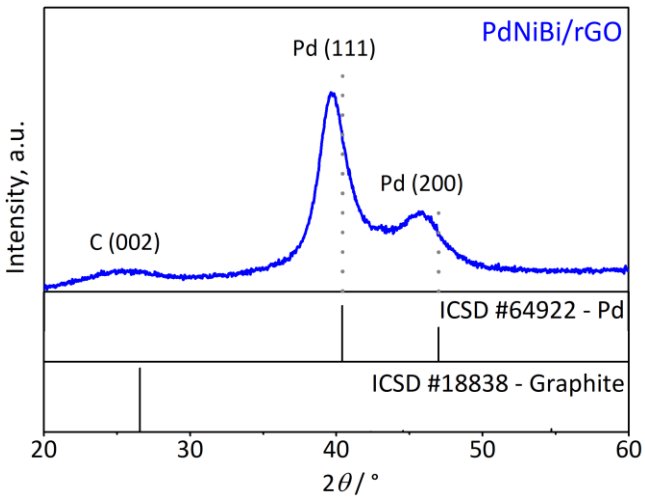

Figure 2. *XRD pattern of PdNiBi/rGO with Pd and graphite ICSD standard data*

The broad peak at a 2θ value of 25.5° can be related to the rGO support material and belongs to the (002) plane of graphite sp^2 carbon structure, signifying the successful synthesis of rGO [8,9,13,16]. The peaks at 2θ values of 39.7 and 43.9° indexed to the (111) and (200) facets, respectively, can be assigned to the face-centered cubic crystalline structure of Pd [8,11]. The shift to lower angles is caused by lattice expansion due to nanosized particles and alloying with Ni and Bi [7,13,15]. The nanocrystalline nature is further indicated by the broad peak shape. The crystallite size of the nanoparticles can be estimated by using the Scherrer equation:

$$D = \frac{k\lambda}{b \cos \theta} \quad (3)$$

where D is the crystallite size (nm), k is the shape factor for spherical particles (0.9), λ refers to the X-ray wavelength (0.154 nm), b is the full width at half maximum of the (111) plane and θ is the half angle [16,17]. The estimated crystallite size was calculated to be approx. 3.8 nm and is in the same range as observed from the TEM analysis.

Electrochemical performance of the EOR catalysts

The electrochemical properties of the PdNiBi/rGO catalyst were investigated by CV and CA measurements and compared with a commercial Pd/C catalyst. The most important results, such as the ECSA and the parameters for the EOR activity and stability, are listed in Table 2.

Table 2. *Electrochemical results of PdNiBi/rGO compared with a commercial Pd/C*

Catalyst	ECSA[a], $cm^2\ mg^{-1}$	E_{onset}[b] / V *vs.* RHE	j_f[c] / mA mg^{-1}	j_b[c] / mA mg^{-1}	j_d[d] / %
PdNiBi/rGO	455.4	0.234	2390	1942	85
Pd/C	410	0.266	2018	2150	87

[a]Electrochemical active surface area; [b]onset potential of the ethanol oxidation at 0.02 mA; [c]peak current density of forward and backward scan; [d]current density decrease after 3600 s.

CVs in de-aerated 1 M KOH electrolyte solution at 10 mV s^{-1} were recorded in a potential range of 0.05 to 1.50 V *vs.* RHE and 0.05 to 1.20 V *vs.* RHE to investigate the oxidation and reduction processes of the materials and to determine the ECSA. The voltammograms are shown in Figure 3.

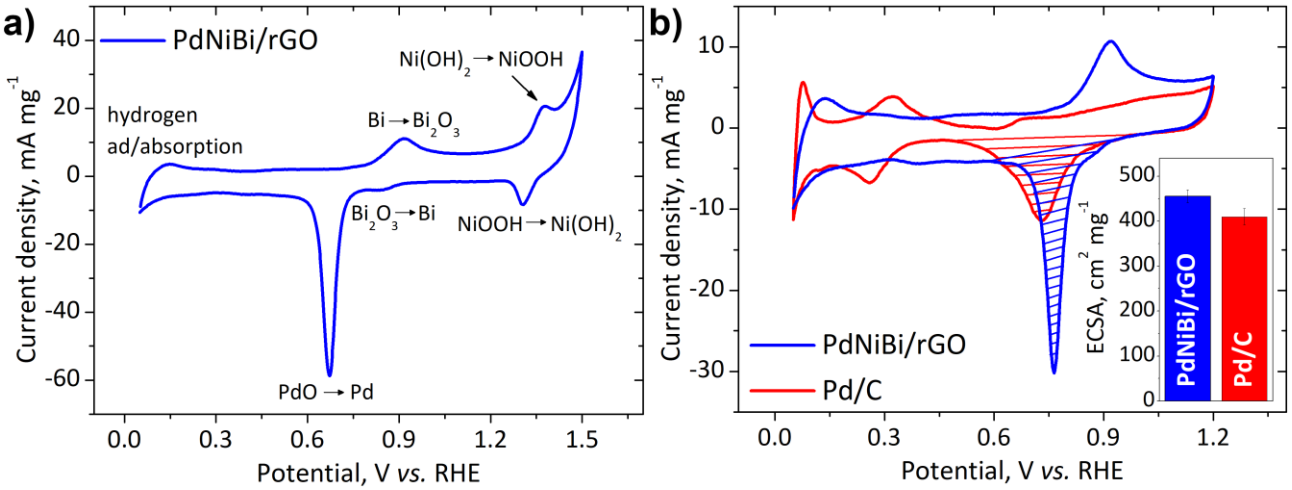

Figure 3. *CV curves in N_2-saturated 1 M KOH electrolyte solution at a scan rate of 10 mV s^{-1} of (a) PdNiBi/rGO in a potential range of 0.05 - 1.50 V* vs. *RHE and (b) PdNiBi/rGO and a commercial Pd/C in a potential range of 0.05 - 1.20 V* vs. *RHE with ECSA evaluation (horizontal segments indicate region for reduction charge determination)*

The CVs of PdNiBi/rGO present that oxidation of Bi to Bi_2O_3 in alkaline media is observed in the anodic scan at approx. 0.9 V *vs.* RHE [18], whereas the oxidation of Pd to PdO is a broad peak, which

is not clearly visible due to overlapping [11]. The peaks between 1.2 to 1.5 V *vs.* RHE describe the oxidation of $Ni(OH)_2$ to NiOOH and the corresponding reduction of NiOOH to $Ni(OH)_2$ (Figure 3a) [19]. The peaks in the cathodic scan between 0.9 V and 0.6 V *vs.* RHE are associated with Bi oxide reduction and the reduction of PdO to Pd [7]. A comparison with the CV (Figure 3b) of the commercial Pd/C shows that the hydrogen ad/absorption peaks for the PdNiBi/rGO are suppressed, which can be attributed to the presence of Bi [18,20,21]. Consequently, the ECSA was estimated from the PdO reduction peak by using equation (4):

$$\text{ECSA} = \frac{Q_{Pd}}{Q^*_{Pd}} \left(\frac{1}{c_L}\right) \left(\frac{1}{A_{GC}}\right) \quad (4)$$

where Q_{Pd} is the determined reduction charge of the PdO to Pd (received using Echem AnalystTM Software-Gamry for baseline correction and integration of the region indicated by horizontal segments), Q^*_{Pd} is the theoretical PdO to Pd reduction charge (405 µC cm^{-2}), c_L is the catalyst loading (56 μg_{Pd} cm^{-2}) and A_{GC} is the GC electrode area (0.196 cm^{-2}) [22-24]. PdNiBi/rGO shows a large ECSA of 455 cm^2 mg^{-1} due to good distribution and small particle size (determined by STEM) as well as the overall high surface area provided by the rGO support [11]. The commercial Pd/C catalyst exhibits an ECSA of 410 cm^2 mg^{-1}. A high ECSA is very important for ensuring high catalytic activity, as it ensures abundant active sites for the ethanol oxidation reaction [25].

The activity of the PdNiBi/rGO catalyst towards EOR was investigated in a mixture of de-aerated 1 M KOH and 1 M EtOH electrolyte solution at a scan rate of 10 mV s^{-1} in a potential range of 0.05 to 1.20 V *vs*. RHE and was compared with the commercial Pd/C catalyst. The CV curves in Figure 4 show two characteristic oxidation peaks, one in the forward and one in the backward scan.

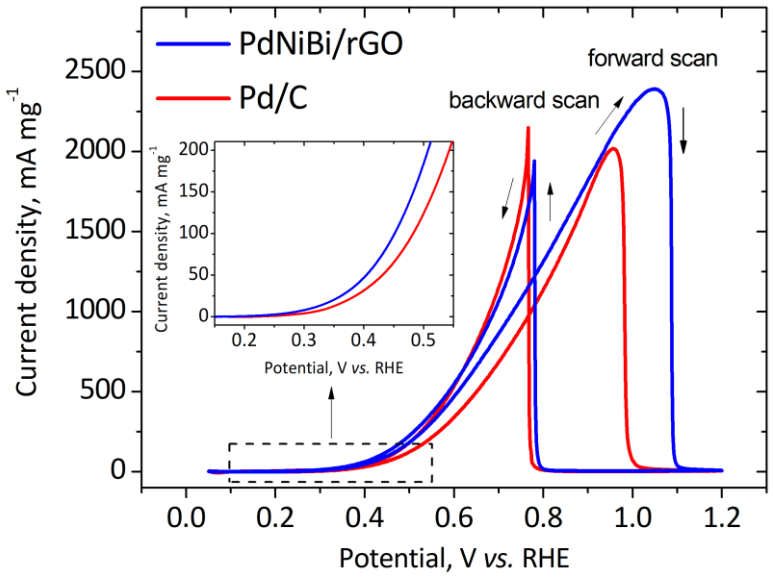

Figure 4. *CV curves of PdNiBi/rGO in N_2-saturated 1 M KOH electrolyte solution containing 1 M EtOH at a scan rate of 10 mV s^{-1} compared with the commercial Pd/C*

The forward peak is attributed to the primary oxidation of ethanol according to the generally accepted EOR reaction mechanism of Pd-based catalysts in alkaline media (equations (5) to (8)) as described by Zhang *et al.* [19] and several other studies [2,26-28]:

$$Pd + CH_3CH_2OH \leftrightarrows Pd - (CH_3CH_2OH)_{ads} \quad (5)$$

$$Pd - (CH_3CH_2OH)_{ads} + 3OH^- \leftrightarrows Pd - (CH_3CO)_{ads} + 3H_2O + 3e^- \quad (6)$$

$$Pd - (CH_3CO)_{ads} + Pd - OH_{ads} \leftrightarrows Pd - CH_3COOH + Pd \quad (7)$$

$$Pd - CH_3COOH + OH^- \leftrightarrows Pd + CH_3COO^- + H_2O \quad (8)$$

In the EOR process, ethanol adsorption and further dissociation (equations (5) and (6)) proceed rapidly in the lower potential region of the anodic scan and the carbonaceous intermediates such as CH_3CO_{ads} will strongly adsorb on the Pd surface. As Pd begins to adsorb OH^- with increased potential, the oxidative removal of the adsorbed carbonaceous species (ascribed as the rate-determining step) happens and the current increases (equations (7) and (8)) [2,19,26,29]. At higher potential, the current rapidly drops when inactive PdO is formed. The backward peak results from the oxidation of freshly adsorbed ethanol molecules after the reduction of the PdO and, thus, recovery of the active sites [8,15,19].

The most important parameters for the activity of an EOR catalyst are the onset potential (E_{onset}), and the maximum peak current density in the forward and backward scan (j_f and j_b). PdNiBi/rGO exhibits an E_{onset} of 0.234 V *vs.* RHE and a j_f and j_b of 2390 mA mg^{-1} and 1942 mA mg^{-1}, respectively. These results are compatible with the literature, *e.g.,* Chowdhury *et al.* [8] described that a j_f of 2223 mA mg^{-1} was obtained with a PdNiP/N-rGO. The EOR activity of PdNiBi/rGO is higher compared to the commercial Pd/C, which is partly caused by the large ECSA generated by the well-distributed, nanosized particles on the rGO support providing abundant active sites [25]. To evaluate the specific activity of the electrocatalysts, the j_f values were normalized by the ECSA. It was found that the PdNiBi/rGO (5.25 mA cm^{-2}) still outperforms the commercial Pd/C (4.92 mA cm^{-2}). Therefore, it can be concluded that not only the higher ECSA but also the presence of the oxophilic elements Ni and Bi additionally ensures the enhancement of the EOR activity, as it has also been shown in other studies in the literature [20,22,24,29]. Ni and Bi are not active for the EOR in the applied potential range, but they have the capability to generate OH_{ads} at the surface at lower potentials due to their oxophilic character. The oxidative desorption of the intermediate carbonaceous species (equation (7)), which is the rate-determining step of the EOR, can thus be facilitated, leading to lower onset potentials and higher current densities [8,15,29,30].

The catalytic stability of the PdNiBi/rGO and commercial Pd/C catalysts towards EOR is determined by performing CA tests in de-aerated 1 M KOH and 1 M EtOH solution for 3600 s. The curves are shown in Figure 5.

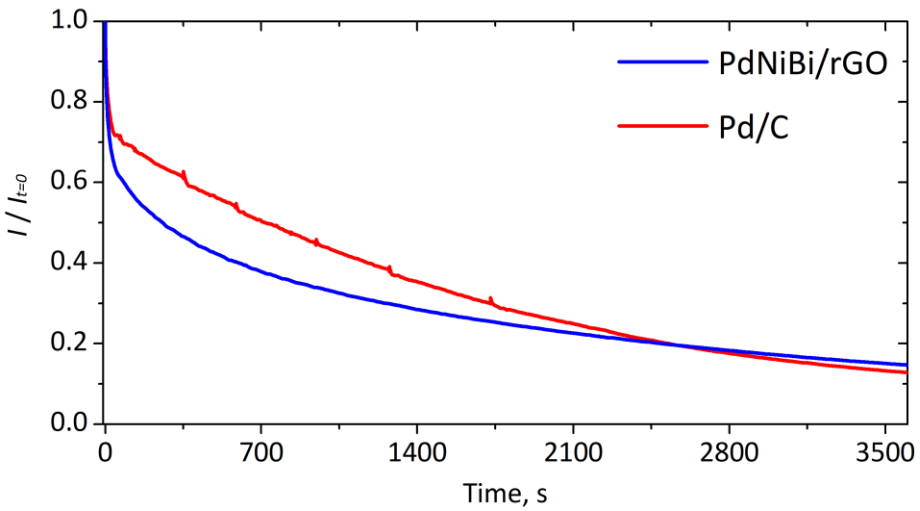

Figure 5. *CA measurement of PdNiBi/rGO and the commercial Pd/C in N_2-saturated 1 M KOH electrolyte solution containing 1 M EtOH at 0.83 V* vs. *RHE*

The current density decrease of EOR catalysts with time can generally be attributed to the poisoning of the active sites on the catalyst metal surface by the adsorption of carbonaceous intermediates (*e.g.,* CH_3CO_{ads}) during ethanol oxidation, as also described in the literature

[8,13,16,29,31]. Lović *et al.* [29] have shown, for example, by recording CVs after the CA, that although the activity is initially lower than before the CA, the loss can be recovered with further cycling. This indicates the stability of the catalyst surface composition and the regeneration of the active sites by the removal of CO-like adsorbates. The results of Figure 5 reveal that PdNiBi/rGO and the commercial Pd/C display a different decrease in current density. Both catalysts exhibit a sharp decay at the beginning, however, the PdNiBi/rGO can then stabilize at a pseudo-steady state condition due to a gradual self-cleaning process [13,29]. The poisonous intermediates can be oxidatively removed by the generation of OH_{ads}, favored by the presence of oxophilic elements (equation (7)) [8,31]. In comparison, the current density of the Pd/C steadily decreases with time as the catalyst is gradually poisoned [8,19]. Therefore, the PdNiBi/rGO composite shows a slightly higher remaining current density after 3600 s than the commercial Pd/C. In summary, the combination of Pd, Ni and Bi with rGO and their synergistic effects proves to be an effective method and highlights the PdNiBi/rGO catalyst as a promising catalyst with high activity and stability for EOR.

Conclusions

In this study, PdNiBi nanoparticles were successfully anchored on a reduced graphene oxide support using the modified instant reduction method. The physicochemical analyses have shown a two-dimensional wrinkled sheet morphology characteristic for graphene-based materials and uniformly and well-distributed metal particles with an average diameter of 2.6 nm on the carbon support caused by strong C-O-M bridges due to the remaining oxygen functionalities of the rGO. The electrochemical tests revealed that the PdNiBi/rGO composite outperformed commercial Pd/C in terms of EOR activity and stability with an ECSA of 455 cm^2 mg^{-1}, an onset potential of 0.234 V *vs.* RHE, a maximum peak current density of 2390 mA mg^{-1} and a current density decrease of 85 % after 3600 s. This enhancement of the electrocatalytic activity could be attributed to the generation of abundant active sites due to the rGO support and the presence of the oxophilic Ni and Bi elements. Based on these physicochemical and electrochemical results, PdNiBi/rGO is highlighted as a promising anode catalyst in alkaline direct ethanol fuel cell applications.

Acknowledgements: *The financial support from the Austrian Science Fund (FWF) [grant number I 3871-N37] in the frame of the project »Graphene Oxide based MEAs for the Direct Ethanol Fuel Cell« and the Slovenian Research Agency (ARRS) through the Research Programms P1-0175, P2-0423, P2-0393 and I0-0003 and the Bilateral Research Funding Projects N2-0087, NC-0007, NC-0016, N2-0155 and N2-0257 are gratefully acknowledged. Special thanks go to Norbert Kienzl for performing the ICP-OES measurements.*

Conflicts of Interest: *The authors declare no conflict of interest.*

References

[1] L. An, T. S. Zhao, Y. S. Li, Carbon-neutral sustainable energy technology: Direct ethanol fuel cells, *Renewable and Sustainable Energy Reviews* **50** (2015) 1462-1468. https://doi.org/10.1016/j.rser.2015.05.074

[2] J. Zhang, Z. Zhao, Y. Wang, J. Wang, D. Peng, B. Li, T. Bo, K. Zheng, Z. Zhou, L. Lv, Z. Xin, B. Zhang, L. Shao, Ethanol electrooxidation on highly active palladium/graphene oxide aerogel catalysts, *Chemical Physics* **534** (2020) 110753. https://doi.org/10.1016/j.chemphys.2020.110753

[3] M. Roschger, S. Wolf, K. Mayer, M. Singer, V. Hacker, Alkaline Direct Ethanol Fuel Cell : Effect of the Anode Flow Field Design and the Setup Parameters on Performance, *Energies* **15** (2022) 7234. https://doi.org/10.3390/en15197234

[4] L. Karuppasamy, S. Anandan, C. Y. Chen, J. J. Wu, Sonochemical Synthesis of PdAg/RGO Nanocomposite as an Efficient Electrocatalyst for Both Ethanol Oxidation and Oxygen Reduction Reaction with High CO Tolerance, *Electrocatalysis* **8** (2017) 430-441. https://doi.org/10.1007/s12678-017-0391-9

[5] S. Wolf, M. Roschger, B. Genorio, M. Kolar, D. Garstenauer, B. Bitschnau, V. Hacker, Ag-MnxOy on Graphene Oxide Derivatives as Oxygen Reduction Reaction Catalyst in Alkaline Direct Ethanol Fuel Cells, *Catalysts* **12** (2022) 780. https://doi.org/10.3390/catal12070780

[6] S. Rezaee, S. Shahrokhian, M. K. Amini. Nanocomposite with Promoted Electrocatalytic Behavior Based on Bimetallic Pd-Ni Nanoparticles, Manganese Dioxide, and Reduced Graphene Oxide for Efficient Electrooxidation of Ethanol, *Journal of Physical Chemistry C* **122** (2018) 9783-9794. https://doi.org/10.1021/acs.jpcc.8b01475

[7] B. Cermenek, B. Genorio, T. Winter, S. Wolf, J. G. Connell, M. Roschger, I. Letofsky-Papst, N. Kienzl, B. Bitschnau, V. Hacker, Alkaline Ethanol Oxidation Reaction on Carbon Supported Ternary PdNiBi Nanocatalyst using Modified Instant Reduction Synthesis Method, *Electrocatalysis* **11** (2020) 203-214. https://doi.org/10.1007/s12678-020-00621-y

[8] S. R. Chowdhury, T. Maiyalagan, S. K. Bhattachraya, A. Gayen, Influence of phosphorus on the electrocatalytic activity of palladium nickel nanoalloy supported on N-doped reduced graphene oxide for ethanol oxidation reaction, *Electrochimica Acta* **342** (2020) 136028. https://doi.org/10.1016/j.electacta.2020.136028

[9] N. Alfi, M. Z. Yazdan-Abad, A. Rezvani, M. Noroozifar, M. Khorasani-Motlagh, Three-dimensional Pd-Cd nanonetwork decorated on reduced graphene oxide by a galvanic method as a novel electrocatalyst for ethanol oxidation in alkaline media, *Journal of Power Sources* **396** (2018) 742-748. https://doi.org/10.1016/j.jpowsour.2018.06.080

[10] J. N. Tiwari, N. K. Dang, H. J. Park, S. Sultan, M. G. Kim, J. Haiyan, Z. Lee, K. S. Kim. Remarkably enhanced catalytic activity by the synergistic effect of palladium single atoms and palladium–cobalt phosphide nanoparticles, *Nano Energy* **78** (2020) 105166. https://doi.org/10.1016/j.nanoen.2020.105166

[11] J. L. Tan, A. M. De Jesus, S. L. Chua, J. Sanetuntikul, S. Shanmugam, B. J. V. Tongol, H. Kim, Preparation and characterization of palladium-nickel on graphene oxide support as anode catalyst for alkaline direct ethanol fuel cell, *Applied Catalysis A* **531** (2017) 29-35. https://doi.org/10.1016/j.apcata.2016.11.034

[12] M. Zhang, J. Xie, Q. Sun, Z. Yan, M. Chen, J. Jing, A. M. S. Hossain. In situ synthesis of palladium nanoparticle on functionalized graphene sheets at improved performance for ethanol oxidation in alkaline media, *Electrochimica Acta* **111** (2013) 855-861. https://doi.org/10.1016/j.electacta.2013.08.135

[13] R. Krishna, D. M. Fernandes, J. Ventura, C. Freire, E. Titus, Facile synthesis of reduced graphene oxide supported Pd@NixB/RGO nanocomposite: Novel electrocatalyst for ethanol oxidation in alkaline media, *International Journal of Hydrogen Energy* **41** (2016) 11811-11822. https://doi.org/10.1016/j.ijhydene.2015.12.034

[14] A. Ručigaj, J. G. Connell, M. Dular, B. Genorio, Influence of the ultrasound cavitation intensity on reduced graphene oxide functionalization, *Ultrasonics Sonochemistry* **90** (2022) 106212. https://doi.org/10.1016/j.ultsonch.2022.106212

[15] M. Roschger, S. Wolf, B. Genorio, V. Hacker, Effect of PdNiBi Metal Content : Cost Reduction in Alkaline Direct Ethanol Fuel Cells, *Sustainability* **14** (2022) 15485. https://doi.org/10.3390/su142215485

[16] K. Bhunia, S. Khilari, D. Pradhan, Monodispersed PtPdNi Trimetallic Nanoparticles-Integrated Reduced Graphene Oxide Hybrid Platform for Direct Alcohol Fuel Cell, *ACS Sustainable Chemistry and Engineering* **6** (2018) 7769-7778. https://doi.org/10.1021/acssuschemeng.8b00721

[17] D. Mahato, T. Gurusamy, S. K. Jain, K. Ramanujam, P. Haridoss, T. Thomas, CuO modified ZnO on nitrogen-doped carbon: a durable and efficient electrocatalyst for oxygen reduction reaction, *Materials Today Chemistry* **26** (2022) 101167. https://doi.org/10.1016/j.mtchem.2022.101167

[18] I. G. Casella, M. Contursi, Characterization of bismuth adatom-modified palladium electrodes. The electrocatalytic oxidation of aliphatic aldehydes in alkaline solutions, *Electrochimica Acta* **52** (2006) 649-657. https://doi.org/10.1016/j.electacta.2006.05.048

[19] Z. Zhang, L. Xin, K. Sun, W. Li, Pd-Ni electrocatalysts for efficient ethanol oxidation reaction in alkaline electrolyte, *International Journal of Hydrogen Energy* **36** (2011) 12686-12697. https://doi.org/10.1016/j.ijhydene.2011.06.141

[20] A. O. Neto, M. M. Tusi, N. S. De Oliveira Polanco, S. G. Da Silva, M. Coelho Dos Santos, E. V. Spinacé, PdBi/C electrocatalysts for ethanol electro-oxidation in alkaline medium, *International Journal of Hydrogen Energy* **36** (2011) 10522-10526. https://doi.org/10.1016/j.ijhydene.2011.05.154

[21] M. Simões, S. Baranton, C. Coutanceau, Influence of bismuth on the structure and activity of Pt and Pd nanocatalysts for the direct electrooxidation of NaBH4, *Electrochimica Acta* **56** (2010) 580-591. https://doi.org/10.1016/j.electacta.2010.09.006

[22] B. Cermenek, J. Ranninger, B. Feketeföldi, I. Letofsky-Papst, N. Kienzl, B. Bitschnau, V. Hacker, Novel highly active carbon supported ternary PdNiBi nanoparticles as anode catalyst for the alkaline direct ethanol fuel cell, *Nano Research* **12** (2019) 683-693. https://doi.org/10.1007/s12274-019-2277-z

[23] S. Jongsomjit, P. Prapainainar, K. Sombatmankhong, Synthesis and characterisation of Pd-Ni-Sn electrocatalyst for use in direct ethanol fuel cells, *Solid State Ionics* **288** (2016) 147-153. https://doi.org/10.1016/j.ssi.2015.12.009

[24] R. N. Singh, A. Singh, Anindita. Electrocatalytic activity of binary and ternary composite films of Pd, MWCNT, and Ni for ethanol electro-oxidation in alkaline solutions, *Carbon* **47** (2009) 271-278. https://doi.org/10.1016/j.carbon.2008.10.006

[25] C. Yao, Q. Zhang, Y. Su, L. Xu, H. Wang, J. Liu, S. Hou, Palladium Nanoparticles Encapsulated into Hollow N-Doped Graphene Microspheres as Electrocatalyst for Ethanol Oxidation Reaction, *ACS Applied Nano Materials* **2** (2019) 1898-1908. https://doi.org/10.1021/acsanm.8b02294

[26] D. Rajesh, P. Indra Neel, A. Pandurangan, C. Mahendiran, Pd-NiO decorated multiwalled carbon nanotubes supported on reduced graphene oxide as an efficient electrocatalyst for ethanol oxidation in alkaline medium, *Applied Surface Science* **442** (2018) 787-796. https://doi.org/10.1016/j.apsusc.2018.02.174

[27] Y. Jin, D. Han, W. Jia, G. Huang, F. Li, X. Chen, R. Li, M. Zheng, W. Gao, B-N Codoped Graphene as a Novel Support for Pd Catalyst with Enhanced Catalysis for Ethanol Electrooxidation in Alkaline Medium, *Journal of The Electrochemical Society* **164** (2017) F638-F644. https://doi.org/10.1149/2.1351706jes

[28] R. C. Cerritos, M. Guerra-Balcázar, R. F. Ramírez, J. Ledesma-García, L. G. Arriaga, Morphological effect of Pd catalyst on ethanol electro-oxidation reaction, *Materials* **5** (2012) 1686-1697. https://doi.org/10.3390/ma5091686

[29] J. D. Lović, V. D. Jović, Electrochemical behaviour of electrodeposited Pd and PdNi coatings for the ethanol oxidation reaction in alkaline solution, *Journal of Electrochemical Science and Engineering* **8** (2018) 39-47. https://doi.org/10.5599/jese.445

[30] S. Y. Shen, T. S. Zhao, J. B. Xu, Y.S. Li, Synthesis of PdNi catalysts for the oxidation of ethanol in alkaline direct ethanol fuel cells, *Journal of Power Sources* **195** (2010) 1001-1006. https://doi.org/10.1016/j.jpowsour.2009.08.079

[31] J. Y. C. Ribeiro, R. S. da Silva, G. R. Salazar-Banda, K. I. B. Eguiluz, Pd-Ni-B/C Nanocatalysts for Electrochemical Oxidation of Ethanol in Alkaline Media, *Catalysis Research* **3** (2023) 005. https://doi.org/10.21926/cr.2301005